

K₃V₂(PO₄)₂F₃ as a robust cathode for potassium ion batteries

Xiuyi Lin, Jiaqiang Huang, Biao Zhang*

Department of Applied Physics, the Hong Kong Polytechnic University, Hung Hom, Hong Kong, China

Email: biao.ap.zhang@polyu.edu.hk

Abstract

Potassium ion batteries (KIBs) have emerged as promising candidates for low-cost and sustainable energy storage systems. The development of KIBs is relatively slow partially due to the large size of potassium ions, rendering great difficulty in designing appropriate host materials. Herein, a K₃V₂(PO₄)₂F₃ cathode is inherited from Na₃V₂(PO₄)₂F₃ analog. The crystallographic structure and phase transformations are unveiled through *in-situ* X-ray diffraction, which shows only minor volume change of 6.2% during potassium ions insertion/extraction. Nearly two potassium ions could be provided by the electrode, delivering a capacity of over 100 mAh g⁻¹ with a high average potential of ~3.7V vs. K⁺/K. An energy density of around 400 Wh kg⁻¹ together with a respectable rate capability have been obtained. Coupling with a graphite anode, a 3.4 Volt-Class battery has been demonstrated, making KIBs promising contenders to sodium ion batteries in large-scale energy storage. This discovery also sheds insights into the quest for potential electrodes from the analogs in Li/Na-ion batteries.

Introduction

The limited amount of lithium sources has raised concerns about the sustainability of Li-ion batteries (LIBs) for the future large-scale application. Alternative batteries based on monovalent Na, K ions and divalent Mg, Ca ions have been booming in recent years to increase the sustainability and reduce the cost.^[1] Similarities between intercalation chemistries of alkali metal ions render significant advantages to the development of Na- and K- ion batteries. Both Na and K elements are much more abundant than Li in the earth crust, potentially decreasing the fabrication cost of batteries. Research on Na- and K- ion batteries (KIBs) could be traced back to 1980s, but the early studies were discouraged by lack of suitable electrode materials. The larger ion size of Na and K than Li imposes challenges on designing appropriate host materials. The revival of Na-ion batteries (NIBs) in the past several years are prompted by the invention of several promising cathodes such as P2-type layered oxides $\text{Na}_{0.67}[\text{Fe}_{0.5}\text{Mn}_{0.5}]\text{O}_2$ ^[2] and polyanionic $\text{Na}_3\text{V}_2(\text{PO}_4)_2\text{F}_3$,^[3] which possess comparable energy densities with the cathodes in LIBs. Nevertheless, the inability of Na ion intercalation in graphite severely restricts the development of anodes. The widely studied hard carbon anodes, in general, deliver much weaker performance than graphite anode in LIBs regarding plateau voltage and tap density. Consequently, the overall energy density of NIBs is around 20% lower than that of LIBs at the current stage.^[4,5] Although having an even larger ion size, it is a delight to find that K ions could be intercalated into graphite to form a stage I graphite intercalation compound KC_8 , as one of the leading advantages of K-ion batteries over NIBs.^[6-8] Moreover, the electrochemical potential of K is lower than Na (-2.93 V for K^+/K and -2.71V for Na^+/Na , both versus standard hydrogen electrode, SHE), suggesting the possibility of building a high voltage cell provided the promising cathode candidates be designed.^[9,10]

Turning to the development of cathodes, an intuitive approach is to design K-based insertion compounds that are analogous to Li and Na counterparts, which has led to the successful synthesis

of Prussian-blue and layered oxides analogs such as $K_xMnFe(CN)_6$ ^[11,12] and $K_{0.7}Fe_{0.5}Mn_{0.5}O_2$.^[13] However, a simple extrapolation is surely not enough considering the structure compatibility as well as the complexity of electrochemical processes. It is clearly reflected in the cases of $K_{0.3}MnO_2$, K_xCoO_2 and $KFeSO_4F$ whose performance, referring to cyclic stability and capacity, is much worse than their Li- and Na-based counterparts.^[14–16] Representing an important category of cathodes, phosphate-based compounds have received great attention due to their structural stability under repeated insertion/extraction. Nevertheless, the few reported candidates are, such as $K_3V_2(PO_4)_3$, failed to show a competitive electrochemical performance with corresponding Li, Na insertion compounds.^[17] Herein, we report a novel fluorophosphate cathode $K_3V_2(PO_4)_2F_3$ derived from $Na_3V_2(PO_4)_2F_3$, which delivers a capacity of over 100 mAh g⁻¹. Coupling with a graphite anode, a full cell having an average voltage of 3.4V is obtained with attractive energy density.

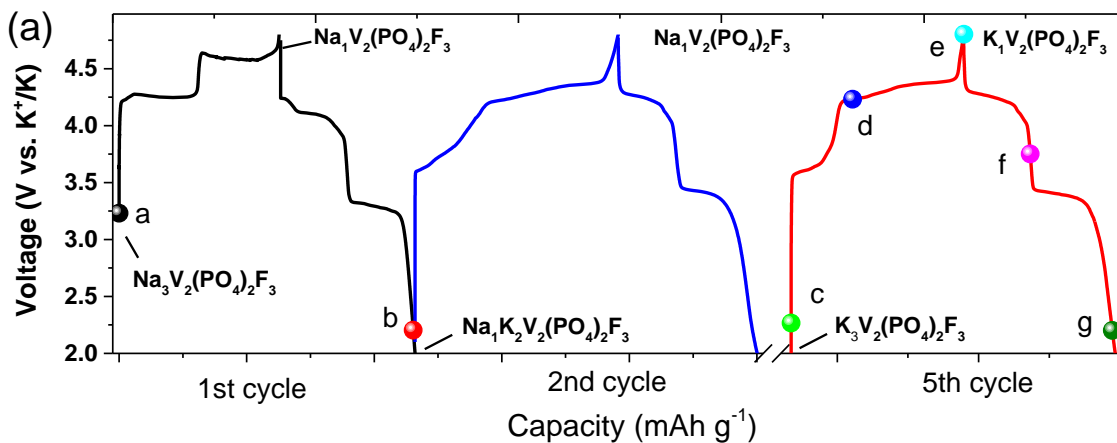
Results and Discussion

Synthesis of $K_3V_2(PO_4)_2F_3$. Inspired by the excellent performance of $Na_3V_2(PO_4)_2F_3$ cathode in NIBs, $K_3V_2(PO_4)_2F_3$ analog is expected to deliver comparable energy densities in KIBs. Attempts in the chemical synthesis of $K_3V_2(PO_4)_2F_3$ were conducted firstly following a similar procedure in preparing $Na_3V_2(PO_4)_2F_3$ without success yet. An electrochemical synthesis strategy through ion exchange was therefore employed making use of $Na_3V_2(PO_4)_2F_3$ as a starting material. The $Na_3V_2(PO_4)_2F_3$ was synthesized by a solid-state reaction according to previous reports.^[18] Afterwards, an electrochemical cell, K metal | 1M KPF_6 in EC/PC | $Na_3V_2(PO_4)_2F_3$, was built to implement Na/K ions exchange. The cell was firstly charged to removed Na ions from $Na_3V_2(PO_4)_2F_3$. Two oxidation plateaus at 4.25 V and 4.60 V are observed as shown in Fig. 1a. The higher charge plateaus of $Na_3V_2(PO_4)_2F_3$ in K cells than that in Na cells (Fig. S1) reside in the redox difference between Na^+/Na (-2.71 V) and K^+/K (-2.93 V). The two plateaus provide a

cumulative capacity of 128 mAh g^{-1} which indicates the successful removal of two Na ions, leaving the $\text{NaV}_2(\text{PO}_4)_2\text{F}_3$ framework. Note that the remaining one Na ion (denoted as the 3rd Na for clear explanation) is considered not accessible due to both kinetic and thermodynamic limitation. Upon discharge, two reduction peaks at 4.25 V and 3.42 V are observed in the voltage profile whose amplitudes suggest the insertion of ~ 1.64 K ions. The following extraction of K ions differs a lot from the extraction of Na ions in the first charge process. A slope at around 3.8V appears firstly followed by a plateau at 4.30V. Along with the cycling, the sloping regime slowly flattens itself to be a plateau at 3.5 V, which remains unchanged starting from the 5th cycle.

The *in-situ* XRD test was conducted to examine the structural evolution during Na/K ions exchanges using a Swagelok cell equipped with an X-ray transparent beryllium window. After the first cycle, the majority of the diffraction peaks shifted to the lower angles (Fig. 1b), which are unfazed considering the larger size of K ions than Na ions. An increase in the crystal lattice is expected after the occupation of K ions on the Na ions sites. Afterwards, the cell was disassembled and the electrode was collected after rinsing with dimethyl carbonate (DMC) to check the K atom contents in the material by energy-dispersive X-ray spectroscopy (EDX). The EDX result gives a K/Na atomic ratio of around 2.3 (Fig. S1a), which is slightly larger than 2.0 in the composition of “ $\text{NaK}_2\text{V}_2(\text{PO}_4)_2\text{F}_3$ ” -- the supposed chemical formula after the exchange of two Na ions with K ions. Since the voltage profiles vary in the first several cycles, we re-examined the crystal structure of electrode when the electrochemical behavior is constant. The diffraction pattern after five cycles (Pattern c in Fig. 1b) is reminiscent of the one after the initial cycle but with the disappearance of some minor peaks. Surprisingly, none of Na atoms has been detected under EDX implying the possible substitution of the 3rd Na by K ion (Fig. S1b). The results are further confirmed by XPS (Fig. S2 and Table S1), which shows a K/V atomic ratio of 1.41 without the appearance of Na

signal. Replacement of the 3rd Na by K ion is out of expectation since it is thought to be inaccessible under the present voltage window. It is speculated that there is a structural reorganization after insertion of two K ions into $\text{Na}_1\text{V}_2(\text{PO}_4)_2\text{F}_3$, during which part of Na and K sites are switched to make the remaining Na available in the following cycles. Previous work indicates a preferred ion migration along the path of three Na sites,^[19] potentially facilitating the structural reorganization. The gradual substitution of the 3rd Na leads to the variation of voltage profiles in the first several cycles, as clearly reflected in the dQ/dV curves (Fig. S3). The curves are stabilized after five cycles when K ions have replaced all the Na ions. Note the the accrate composition is difficult to be determined here due to the presence of solid electrolyte interphase (SEI). According to the XPS results, the formula could be roughly expressed as $\text{K}_{3-x}\text{V}_2(\text{PO}_4)_2\text{F}_3$ ($0 < x < 1$) (Table S1). For sake of conciseness, the material is denoted as $\text{K}_3\text{V}_2(\text{PO}_4)_2\text{F}_3$ afterwards.



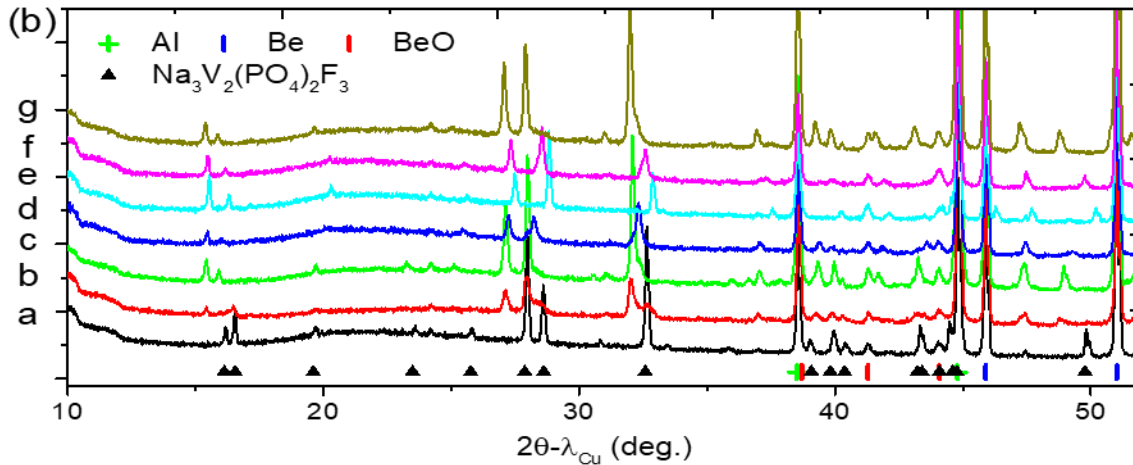


Fig.1 (a) Voltage profiles of de-sodiation of $\text{Na}_3\text{V}_2(\text{PO}_4)_2\text{F}_3$ and the following potassiation/depotassiation; (b) *In-situ* XRD patterns collected at different stages marked in (a).

The structure evolution during K ions insertion/extraction in $\text{K}_3\text{V}_2(\text{PO}_4)_2\text{F}_3$ was further analyzed by Rietveld refinement to investigate the corresponding phase change. It is reported that the $\text{Na}_3\text{V}_2(\text{PO}_4)_2\text{F}_3$ (space group $A_{\text{m}}\text{am}$) undergoes a phase transformation to $\text{Na}_2\text{V}_2(\text{PO}_4)_2\text{F}_3$ (Space group $I4/m\text{m}\text{m}$) after the first plateau and further to $\text{Na}_1\text{V}_2(\text{PO}_4)_2\text{F}_3$ (Space group $\text{Cm}c2_1$) as a final phase in the oxidation.^[18] XRD refinement was performed using the similar structural model with $\text{Na}_3\text{V}_2(\text{PO}_4)_2\text{F}_3$ but replacing Na ions by K ions. A good fitting between the observed and calculated patterns is obtained using the proposed $\text{K}_3\text{V}_2(\text{PO}_4)_2\text{F}_3$ structure (Fig. 2a). $\text{K}_3\text{V}_2(\text{PO}_4)_2\text{F}_3$ has a volume of 938.78 \AA^3 for the unit cell (Table S2) and is larger than 878.05 \AA^3 for $\text{Na}_3\text{V}_2(\text{PO}_4)_2\text{F}_3$ ^[20] because of the bigger size of K ion than Na ion. Around 0.6 K ion is extracted when charging to 4.2V, giving rise to an approximate composition of $\text{K}_2\text{V}_2(\text{PO}_4)_2\text{F}_3$. A decent refinement results are obtained showing a lattice parameter of $a = b = 6.336(1) \text{ \AA}$, $c = 11.506(3) \text{ \AA}$ (Fig. S4a, Table S3). Further oxidation leads to the removal of another ~ 1.0 K ion to give a chemical formula of $\text{K}_1\text{V}_2(\text{PO}_4)_2\text{F}_3$, which agrees well with the $\text{Cm}c2_1$ structure model. The formed

phase after charging to 4.6 V has a unit cell volume of 884.65 \AA^3 . (Fig. S4b and Table S4). The overall volume change from $\text{K}_3\text{V}_2(\text{PO}_4)_2\text{F}_3$ to $\text{K}_1\text{V}_2(\text{PO}_4)_2\text{F}_3$ is only $\Delta V/V=6.2\%$, as calculated in Fig. S4c. As a reference, the prestigious polyanionic cathode LiFePO_4 undergoes a volume change of 7.0% during Li insertion/extraction. The even smaller value obtained for $\text{K}_3\text{V}_2(\text{PO}_4)_2\text{F}_3$ implies the stability of the electrodes for long-term cycles. The cells were then disassembled and washed to collect $\text{K}_3\text{V}_2(\text{PO}_4)_2\text{F}_3$ powders for evaluating their electrochemical properties in Na ions free environment.

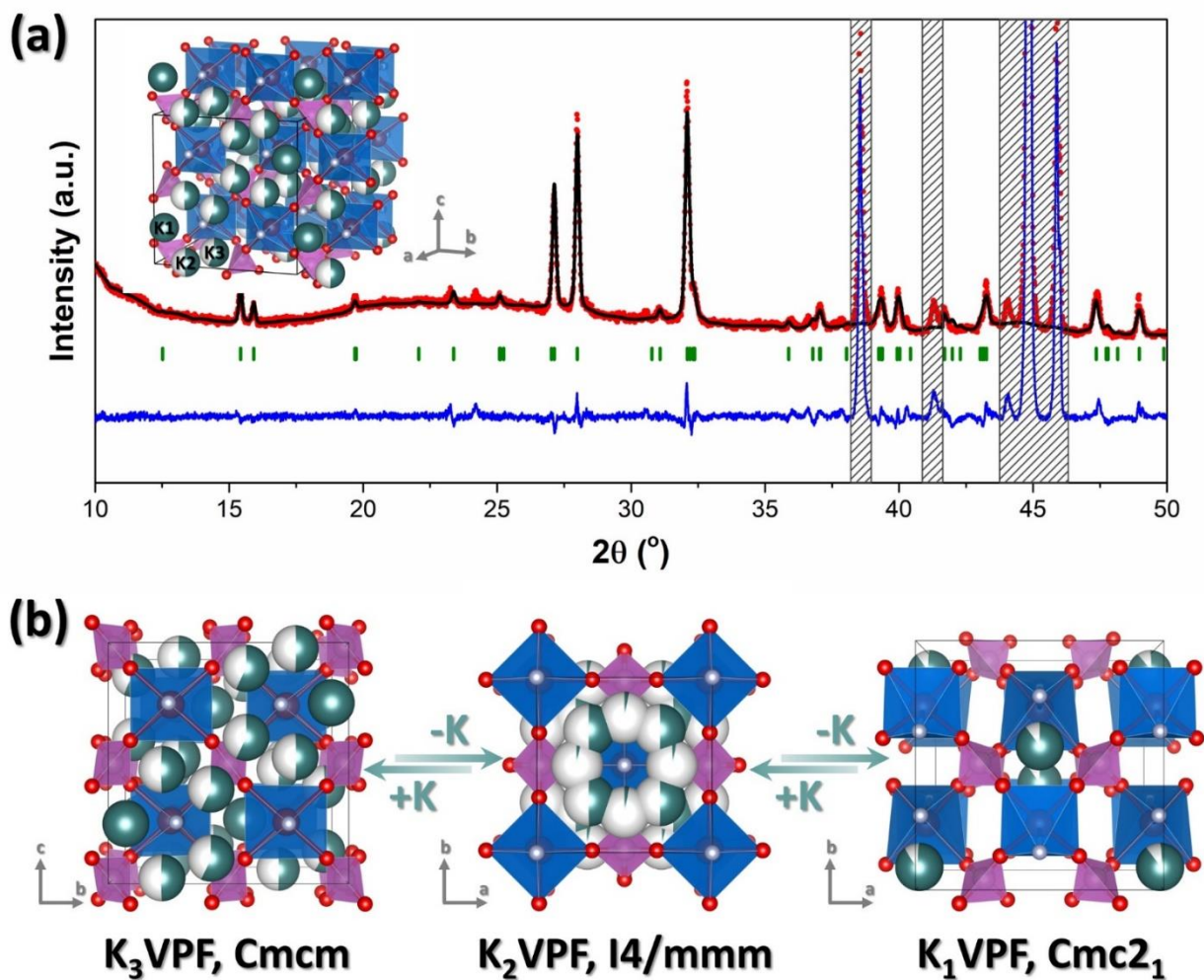


Fig.2 (a) Rietveld refinement of $\text{K}_3\text{V}_2(\text{PO}_4)_2\text{F}_3$, the red points, black lines and bottom blue lines denote the experimental, calculated and difference patterns; Vertical tic bars give the diffraction

peaks from proposed Cmcm groups. The shadow areas are the peaks from Be, BeO, and Al foils.

(b) Phase transformation during K ion insertion and extraction. VO₄F₂ octahedral and PO₄ tetrahedral are labeled in blue and purple, respectively. K atoms are in cyan, where the white part indicate vacancies.

Electrochemical performance of K₃V₂(PO₄)₂F₃. The electrochemical performance was examined in coin cells with a piece of potassium metal as both counter and reference electrode and 1 M KPF₆ in EC/PC as the electrolyte. The cells were firstly tested at a current density of 10 mA g⁻¹ (around 0.1 C) between 2.0-4.6V. Fig.3a shows the corresponding voltage-capacity profiles, which consist of two plateaus in both charge and discharge curves. A close examination through dQ/dV derivative curves (inset of Fig. 3a) reveal that each plateau comprises two sub-plateaus, which are very close to each other, i.e., 3.43 and 3.48 V for the lower voltage one, 4.30 and 4.16 V for the higher voltage one. The observations indicate the complexities of the intermediate phases among K_{3-x}V₂(PO₄)₂F₃ (0≤x≤2) family, similar to the cases in Na_{3-x}V₂(PO₄)₂F₃ where a series of phases like Na_{2.4}V₂(PO₄)₂F₃ and Na_{1.3}V₂(PO₄)₂F₃ have been discovered.^[18] High-resolution diffraction patterns through synchrotron radiation are required in the future studies to unveil the precise composition and atom sites in K-based counterparts. The four plateaus contribute a cumulative capacity of 104 mAh g⁻¹ with an average potential of 3.7 V vs. K⁺/K. Subsequent charge/discharge curves follow almost identically the traces of initial one, confirming the excellent reversibility of the electrode.

The current densities were gradually increased to test the rate capability. A general concern towards the K-ion batteries is the large size of K ions, which may bring about the slow kinetic issue under high currents. Notably, 80% retention of the capacity is maintained when the current

density increased from 10 to 100 mA g⁻¹ for K₃V₂(PO₄)₂F₃, i.e., 83 mAh g⁻¹. Even under 250 mA g⁻¹ (~2C), a relatively high capacity of 50 mAh g⁻¹ is left. The outstanding rate capacity is attributed to the open framework constructed by VO₄F₂ octahedral and PO₄ tetrahedral (Fig. 2b), inheriting from Na₃V₂(PO₄)₂F₃ frame. It is worth mentioning that K₃V₂(PO₄)₂F₃ prepared here has a large size of ~ 2 μm (Fig. S5). The rate capability could be further improved through the preparation of nanosized particles. Furthermore, the capacity is recovered to 101 mAh g⁻¹ when the current density returns to 10 mA g⁻¹, possessing a capacity retention of 97% for 100 cycles.

Overall, the K₃V₂(PO₄)₂F₃ delivers an energy density of 385 Wh kg⁻¹, which outperforms almost all the potassium-based layered oxides and polyanionic cathodes developed until now (Fig. 3c). Compared to another promising fluorophosphate cathode KVPO₄F, as-prepared K₃V₂(PO₄)₂F₃ holds the advantage of appropriate voltage range for safe operation. A charge potential up to 5V is required in KVPO₄F to realize its capacity, which triggers copious electrolyte decomposition. The energy density of K₃V₂(PO₄)₂F₃ currently only falls behind the recent reported Prussian type cathodes. Nevertheless, the gap between them could be significantly narrowed if the capacity of K₃V₂(PO₄)₂F₃ is fully utilized. According to the final oxidized phase of K₁V₂(PO₄)₂F₃, two K ions should be available for delivering a capacity of 115 mAh g⁻¹ theoretically. Efforts are taking to optimize the crystallography and microstructure to reach this value, which will be a competitive cathode for the up-coming KIB technologies.

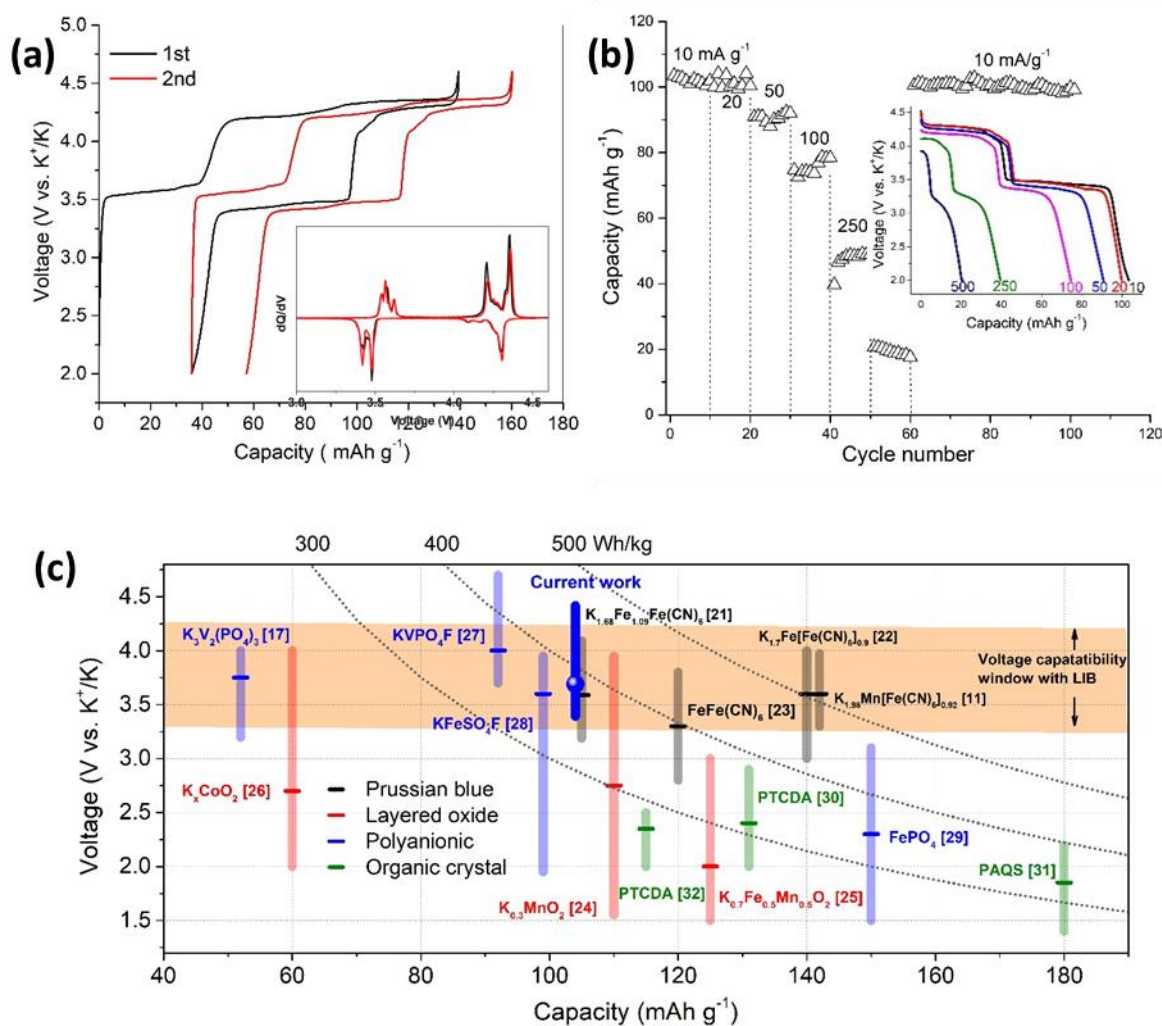


Fig.3 (a) Voltage profiles of $\text{K}_3\text{V}_2(\text{PO}_4)_2\text{F}_3$ in the initial two cycles. The inset shows the corresponding dQ/dV curves. (b) Rate capability of the material and its discharge curves under various current densities; (c) Compassion of the voltage and capacities of as-prepared $\text{K}_3\text{V}_2(\text{PO}_4)_2\text{F}_3$ with different types of cathodes reported until now: Prussian blue ^[11,21–23], Layered oxides ^[13,15,24], Polyanionic ^[17,25,14,26] and organic crystal ^[27–29].

Full cells demonstration. The $\text{K}_3\text{V}_2(\text{PO}_4)_2\text{F}_3$ was matched with a graphite anode to demonstrate the feasibility of building K-ion full cells. Utilization of graphite as an anode is among one of the

advantages of KIBs over NIBs. The very mature graphite-production technologies developed in LIBs will greatly facilitate the commercialization process of KIBs. The graphite adopted here possess a reversible capacity of 220 mAh g^{-1} with an average potential of $\sim 0.35 \text{ V}$ (Fig. S6), thereby enabling us to design a 3.40 Volt-class KIB. The amount of graphite is 5% in excess when coupling with the $\text{K}_3\text{V}_2(\text{PO}_4)_2\text{F}_3$ to avoid the possible K metal plating. The full cell delivers an initial charge capacity of 126 mAh g^{-1} and a discharge capacity of 84 mAh g^{-1} , showing a coulombic efficiency of 67% (Fig. 4). The irreversible capacity mainly comes from the SEI formation on the graphite side, calling for the design of “K reservoirs” to compensate the K ions loss.^[20] The coulombic efficiency gradually increases but the first ten cycles possess a low value of $<96\%$, resulting in the fast capacity fading. Future studies on modification of graphite surface and optimization of the electrolyte are necessary to construct stable electrolyte-electrode interphases on both anode and cathode sides. Nevertheless, the capacity is stabilized after ten cycles, and a capacity of 59 mAh g^{-1} is maintained for 50 cycles (the inset of Fig. 4). The observation proves the potential of KIBs as alternatives for low-cost, sustainable energy storage.

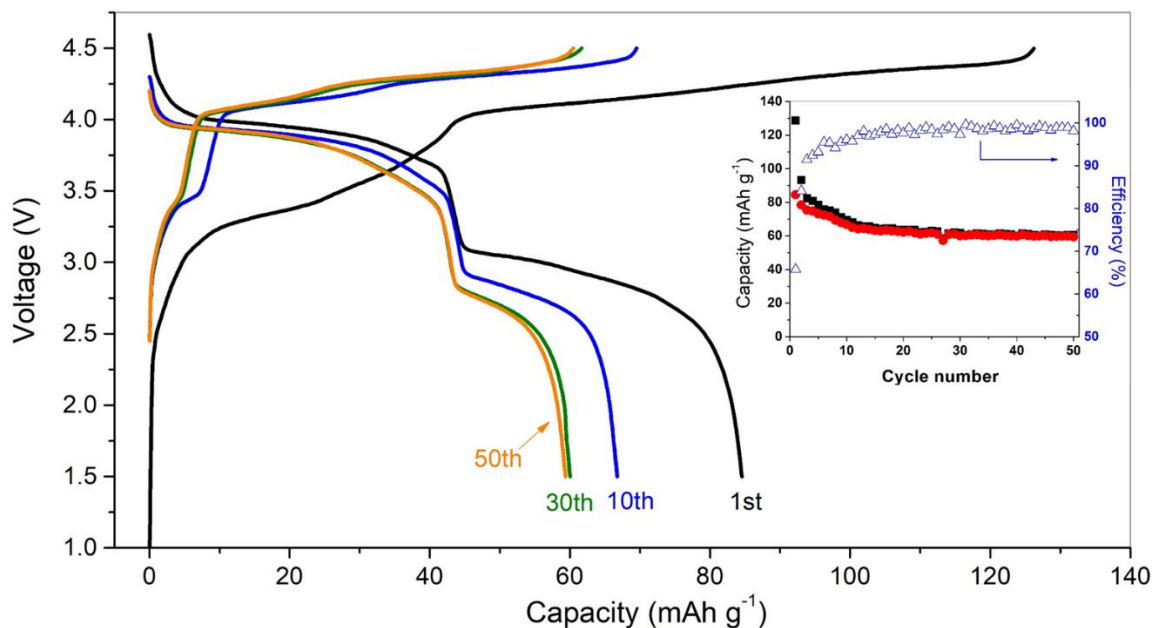


Fig.4 The charge/discharge curves of a full K-ion cell where a graphite anode is used. The inset gives the cyclic performance of the cell.

Conclusions

A novel polyanionic cathode $\text{K}_3\text{V}_2(\text{PO}_4)_2\text{F}_3$ have been synthesized based on $\text{Na}_3\text{V}_2(\text{PO}_4)_2\text{F}_3$ analog. It shows a high average voltage of 3.7 V and a capacity of over 100 mAh g^{-1} , making it among the most competitive cathodes for KIBs. *In-situ* XRD has been employed to unravel the phase transformation during reversible K ion insertion and extraction. A small volume change (6.2%) occurs during cycling, explaining for long-term cyclic stability. The performance is further evaluated in full cells coupling with a graphite anode, successfully demonstrating the feasibility of assembling a 3.4 Volt-class KIB with a decent performance. Several optimizations ranging from electrolyte compatibility to microstructure design of the electrode material are apparent to fully explore its capacity. The findings also have substantial implications in searching for potential electrodes from Li- and Na- analogs, thereby speeding up the development of high-performance KIBs.

References:

- [1] D. Larcher, J. Tarascon, *Nat. Chem.* **2014**, *7*, 19–29.
- [2] N. Yabuuchi, M. Kajiyama, J. Iwatate, H. Nishikawa, S. Hitomi, R. Okuyama, R. Usui, Y. Yamada, S. Komaba, *Nat. Mater.* **2012**, *11*, 512–517.
- [3] Y.-U. Park, D.-H. Seo, H. Kim, J. Kim, S. Lee, B. Kim, K. Kang, *Adv. Funct. Mater.* **2014**, *3*, n/a-n/a.
- [4] V. Palomares, P. Serras, I. Villaluenga, K. B. Hueso, J. Carretero-González, T. Rojo, *Energy Environ. Sci.* **2012**, *5*, 5884.
- [5] D. Kundu, E. Talaie, V. Duffort, L. F. Nazar, *Angew. Chemie Int. Ed.* **2015**, *54*, 3431–3448.
- [6] J. Zhao, X. Zou, Y. Zhu, Y. Xu, C. Wang, *Adv. Funct. Mater.* **2016**, *26*, 8103–8110.
- [7] W. Luo, J. Wan, B. Ozdemir, W. Bao, Y. Chen, J. Dai, H. Lin, Y. Xu, F. Gu, V. Barone, et al., *Nano Lett.* **2015**, *15*, 7671–7677.
- [8] Z. Jian, W. Luo, X. Ji, *J. Am. Chem. Soc.* **2015**, *137*, 11566–11569.
- [9] H. Kim, J. C. Kim, M. Bianchini, D.-H. Seo, J. Rodriguez-Garcia, G. Ceder, *Adv. Energy Mater.* **2017**, *1702384*, 1702384.
- [10] X. Wu, D. P. Leonard, X. Ji, *Chem. Mater.* **2017**, *29*, 5031–5042.
- [11] L. Xue, Y. Li, H. Gao, W. Zhou, X. Lü, W. Kaveevivitchai, A. Manthiram, J. B. Goodenough, *J. Am. Chem. Soc.* **2017**, *139*, 2164–2167.
- [12] X. Bie, K. Kubota, T. Hosaka, K. Chihara, S. Komaba, *J. Mater. Chem. A* **2017**, *5*, 4325–4330.
- [13] X. Wang, X. Xu, C. Niu, J. Meng, M. Huang, X. Liu, Z. Liu, L. Mai, *Nano Lett.* **2016**, *acs.nanolett.6b04611*.
- [14] N. Recham, G. Rousse, M. T. Sougrati, J. N. Chotard, C. Frayret, S. Mariyappan, B. C. Melot, J. C. Jumas, J. M. Tarascon, *Chem. Mater.* **2012**, *24*, 4363–4370.

- [15] Y. Hironaka, K. Kubota, S. Komaba, *Chem. Commun.* **2017**, 53, 3693–3696.
- [16] C. Vaalma, G. A. Giffin, D. Buchholz, S. Passerini, *J. Electrochem. Soc.* **2016**, 163, A1295–A1299.
- [17] J. Han, G.-N. Li, F. Liu, M. Wang, Y. Zhang, L. Hu, C. Dai, M. Xu, *Chem. Commun.* **2017**, 53, 1805–1808.
- [18] M. Bianchini, F. Fauth, N. Brisset, F. Weill, E. Suard, C. Masquelier, L. Croguennec, *Chem. Mater.* **2015**, 27, 3009–3020.
- [19] I. L. Matts, S. Dacek, T. K. Pietrzak, R. Malik, G. Ceder, *Chem. Mater.* **2015**, 27, 6008–6015.
- [20] B. Zhang, R. Dugas, G. Rousse, P. Rozier, A. M. Abakumov, J.-M. Tarascon, *Nat. Commun.* **2016**, 7, 10308.
- [21] X. Wu, Z. Jian, Z. Li, X. Ji, *Electrochem. commun.* **2017**, 77, 54–57.
- [22] G. He, L. F. Nazar, *ACS Energy Lett.* **2017**, 2, 1122–1127.
- [23] Z. Shadike, D.-R. Shi, T.-W. Tian-Wang, M.-H. Cao, S.-F. Yang, J. Chen, Z.-W. Fu, *J. Mater. Chem. A* **2017**, 5, 6393–6398.
- [24] C. Vaalma, G. A. Giffin, D. Buchholz, S. Passerini, *J. Electrochem. Soc.* **2016**, 163, A1295–A1299.
- [25] K. Chihara, A. Katogi, K. Kubota, S. Komaba, *Chem. Commun.* **2017**, 53, 5208–5211.
- [26] V. Mathew, S. Kim, J. Kang, J. Gim, J. Song, J. P. Baboo, W. Park, D. Ahn, J. Han, L. Gu, et al., *NPG Asia Mater.* **2014**, 6, e138.
- [27] Y. Chen, W. Luo, M. Carter, L. Zhou, J. Dai, K. Fu, S. Lacey, T. Li, J. Wan, X. Han, et al., *Nano Energy* **2015**, 18, 205–211.
- [28] Z. Jian, Y. Liang, I. A. Rodríguez-Pérez, Y. Yao, X. Ji, *Electrochem. commun.* **2016**, 71, 5–

8.

- [29] Z. Xing, Z. Jian, W. Luo, Y. Qi, C. Bommier, E. S. Chong, Z. Li, L. Hu, X. Ji, *Energy Storage Mater.* **2016**, 2, 63–68.